

What Causes Optical Flow Networks to be Vulnerable to Physical Adversarial Attacks

Simon Schrodi Tonmoy Saikia Thomas Brox

University of Freiburg, Germany

{schrodi, saikiat, brox}@cs.uni-freiburg.de

Abstract

Recent work demonstrated the lack of robustness of optical flow networks to physical, patch-based adversarial attacks. The possibility to physically attack a basic component of automotive systems is a reason for serious concerns. In this paper, we analyze the cause of the problem and show that the lack of robustness is rooted in the classical aperture problem of optical flow estimation in combination with bad choices in the details of the network architecture. We show how these mistakes can be rectified in order to make optical flow networks robust to physical, patch-based attacks.

1. Introduction

While deep learning has been conquering many new application domains, it has become more and more evident that deep networks are vulnerable to distribution shifts. A particular way to showcase this vulnerability is adversarial attacks, where one finds the minimal input perturbation that is sufficient to falsify the network output. As the small targeted perturbation moves the sample out of the training distribution, the network is detached from its learned patterns and follows the suggestive pattern of the attack. Although many methods have been proposed to improve robustness [38], they only alleviate the problem but do not solve it [1].

While most white-box adversarial attacks are mainly of academic relevance as they reveal the weaknesses of deep networks w.r.t. out-of-distribution data, physical adversarial attacks have serious consequences for safe deployment. In physical attacks, the input is not perturbed artificially, but a confounding pattern is placed in the real-world to derail the machine learning approach.

Most work on adversarial attacks has been concerned with recognition problems, and it looked for a while as if correspondence problems are not a good target for adversarial attacks. However, Ranjan *et al.* [28] showed that they can successfully perform a physical attack on optical flow



Figure 1: **Overview.** Physical, patch-based adversarial attacks on optical flow can be avoided by minor architectural changes. First row: attacked first frame. Second row: ground truth optical flow. Third and fourth rows: the resulting optical flow estimates of FlowNetC [9] and our proposed Robust FlowNetC. FlowNetC is strongly affected by the adversarial patch, whereas Robust FlowNetC is barely affected. For the robust version we make simple design changes based on causes of the attack; see Section 6.

networks. They optimized an adversarial local patch that they can paste into both images, such that large errors appear in the estimated optical flow field even far away from the affected image location. The same adversarial patch worked for multiple architectures. They demonstrated even physical attacks, where the printed patch is physically added to a scene and derails the optical flow estimation. Ranjan *et al.* found that different network architectures show different levels of vulnerability, whereas conventional optical flow methods are not vulnerable at all. They hypothesized the cause for the vulnerability to be in the common encoder-decoder architecture of FlowNet [9] and its derivatives, but did not provide a conclusive analysis.

In this paper, we finish their work by a deeper analysis for the actual cause of the vulnerability to patch-based adversarial attacks on optical flow. In particular, we answer

the following questions.

- (1) What is the true cause of a successful attack?
- (2) Knowing the cause, can the attack also be built without optimizing it for the particular network (zero query black-box attack)?
- (3) Can the severe vulnerability be avoided by a specific design of the network architecture or by avoiding mistakes in such design?

2. Related Work

Optical flow. For many decades, optical flow was estimated with approaches that minimize an energy consisting of a matching cost and a term that penalizes deviation from smoothness [16, 4, 6, 7].

Inspired by the success of CNNs on recognition tasks, Dosovitskiy *et al.* [9] introduced estimation of optical flow with a deep network, by training it end-to-end. They proposed two network architectures - FlowNetS and FlowNetC - of which the first is a regular encoder-decoder architecture, whereas the second includes an additional correlation layer that explicitly computes a cost volume for feature correspondences between the two images – like the correlation approaches from the very early days of optical flow estimation, but integrated in the surrounding of a deep network for feature learning and interpretation of the correlation output. The concept of these architectures has been picked up by many follow-up works that introduced, for instance, coarse-to-fine estimation [27, 31], stacking [17], and multi-scale 4D all-pairs correlation volumes combined with the separate use of a context encoder as well as a recurrent unit for iterative refinement [34]. Most of the architectures have an explicit correlation layer like the original FlowNetC.

Adversarial attacks. The first works that brought up the issue of vulnerability of deep networks to adversarial samples were in the context of image classification and generated the samples by solving a box-constrained optimization problem [33] or by perturbing the input images with the gradient w.r.t. the input [12]. Su *et al.* [30] showed that neural networks can be even attacked by just changing a single pixel. Kurakin *et al.* [18] showed that adversarial attacks also work in the physical world by printing out adversarial examples. Several follow-up works have confirmed this behavior in other contexts [5, 10, 3]. Hendrycks *et al.* [15] showed that adversarial examples can even exist in natural, unmodified, real-world images, which relates adversarial attacks to the more general issue with out-of-distribution samples.

Several works have proposed methods for empirical defenses against adversarial attacks [18, 24, 21, 26], yet other works have shown that these defenses can be circumvented, implying there is a cat-and-mouse game between defenses and potential new kinds of adversarial attacks [1, 2, 8, 35].

Works on adversarial attacks concentrated on various sorts of recognition tasks, *i.e.*, tasks where the output depends directly on some feature representation of the input image, such as classification, semantic segmentation, single-view depth estimation, or image retrieval. Recently, Ranjan *et al.* [28] showed that also optical flow networks are vulnerable to patch-based adversarial attacks and can also attack flow networks in a real world setting. From their experimental evidence, they hypothesized that the encoder-decoder architecture is the main cause for the adversarial vulnerability, whereas spatial pyramid architectures as well as classical optical flow approaches are more robust to adversarial attacks. Further they showed that flow networks are not spatially invariant and the deconvolutional layers lead to an amplification of activations as well as checkerboard artifacts [25]. Recently, Wong *et al.* [37] showed that imperceptible perturbations added to each pixel individually can significantly deteriorate the output of stereo networks. However, these global perturbations can hardly be used for physical attacks. In this paper, we therefore focus our study on patch-based adversarial attacks [28] rather than globally applied perturbations [37].

3. Patch-based Adversarial Attacks on Optical Flow

In this section we briefly discuss background work on patch-based adversarial attacks on optical flow and robustness of existing optical flow approaches towards such attacks.

Adversarial patch. Ranjan *et al.* [28] proposed attacking the network by pasting a patch p of resolution $h \times w$ onto the image frames $(I_t, I_{t+1}) \in \mathcal{I}$ of resolution $H \times W$ at the same location, rotation and scaling. To determine the optimal patch, they minimize the cosine similarity between the unattacked flow (u, v) and the attacked one (\tilde{u}, \tilde{v}) computed with flow network F . More formally, they optimize

$$\hat{p} = \underset{p}{\operatorname{argmin}} \mathbb{E}_{(I_t, I_{t+1}) \sim \mathcal{I}, l \sim \mathcal{L}, \delta \sim \mathcal{T}} \frac{(u, v) \cdot (\tilde{u}, \tilde{v})}{\|(u, v)\| \cdot \|(\tilde{u}, \tilde{v})\|}, \quad (1)$$

where they randomly sample the location $l \in \mathcal{L}$ and affine transformations $\delta \in \mathcal{T}$, *i.e.*, rotation and scaling, to generalize better to a real world setting.

Impact of correct data normalization. In the typical deep learning setting, we normalize the input data in the preprocessing step, as this usually leads to faster convergence [19]. Since we use data normalization for training, we must also use the same data normalization during inference, since the model learns based on these normalized inputs. Using the wrong data normalization usually has a detrimental effect on performance.



Figure 2: **The use of different data normalizations lead to different results for FlowNetC.** We optimize and evaluate a 102×102 patch for each data normalization. Visualizations from left to right: the attacked first frame, the unattacked flow estimate, the attacked flow estimate, the difference between the attacked and unattacked optical flow estimates. Best viewed in color and with zoom.

Network	Un- attacked EPE	Attacked	
		102x102 (2.1%)	153x153 (5.8%)
FlowNetC as [28]	14.52	94.51	197.00
FlowNetC as [17]	11.50	52.66	51.99
FlowNetS [9]	14.33	17.35	17.92
FlowNet2 as [28]	11.82	27.59	43.14
FlowNet2 as [17]	10.07	12.40	13.36
SPyNet [27]	24.26	27.47	25.84
PWC-Net [31]	12.55	18.08	17.70
RAFT [34]	5.86	8.48	9.01

Table 1: **Attacks on different flow networks.** We show average unattacked and average worst case attacked EPE on the KITTI 2015 training dataset (for details see Section 4). We only show the largest patch sizes, since smaller patches show simply a weaker effect [28].

We found that Ranjan *et al.* [28] normalize inputs of FlowNetC and FlowNet2 to the interval $[-1, 1]$, which is different from the data normalization FlowNetC and FlowNet2 use during training. More specifically, Ilg *et al.* [17] first normalize inputs to $[0, 1]$ and then subtract the mean of each RGB channel computed during the first 1000 iterations in training. As a result, FlowNetC’s and FlowNet2’s unattacked and attacked End-Point-Error (EPE) on the KITTI 2015 training dataset [23] drop significantly (see Figure 2 and Table 1). However, despite this correction of the normalization, FlowNetC is still vulnerable, so the result of Ranjan *et al.* [28] is still valid.

Vulnerability of existing optical flow methods. Ranjan *et al.* [28] found that different network architectures show different vulnerability. Table 1 shows the vulnerability for different architectures for patches of size 102×102 and 153×153 . While some networks, especially FlowNetC, suffer a lot from the attack, others like PWC-Net, SPyNet

and RAFT are much less vulnerable. Note that since there is no motion within the patch, we modify the ground truth in this area to zero flow.

Ranjan *et al.* [28] attributed the vulnerability to the encoder-decoder architecture and the higher robustness to the spatial pyramid of PWC-Net and SpyNet. However, FlowNetS does not use a spatial pyramid. It is a plain encoder-decoder architecture and, as Table 1 reveals, it is quite robust to the attack. Thus, the encoder-decoder architecture cannot be the root cause for the vulnerability to adversarial attacks, even though the decoder can be responsible for amplifying the effect.

4. What is the True Cause of a Successful Patch-based Attack?

In this section, we conduct a thorough analysis in the quest for the actual cause of the vulnerability to adversarial attacks. We build on the attack procedure of Ranjan *et al.* [28] and also use KITTI 2012 [11] for patch optimization. For evaluation, we also use their white-box evaluation procedure on KITTI 2015 [23]. We show the importance of the spatial location as well as analyze the flow networks’ feature embeddings. Through this analysis, we can trace the adversarial attacks back to the classical aperture problem in optical flow. For sake of brevity, we mostly focus on FlowNetC, since it is the most vulnerable flow network, as well as PWC-Net and RAFT.

4.1. Spatial Location Heat Map

We analyze the impact of the spatial location of the adversarial patch by placing the adversarial patch at different locations in the image and computing the attacked EPE for each location. For visualizations of the resulting heat map, we linearly interpolate between values and clip them. Our experiment allows us to identify three potential attacking scenarios: best case, median case, and worst case. For example, in the worst case scenario, we paste the patch at

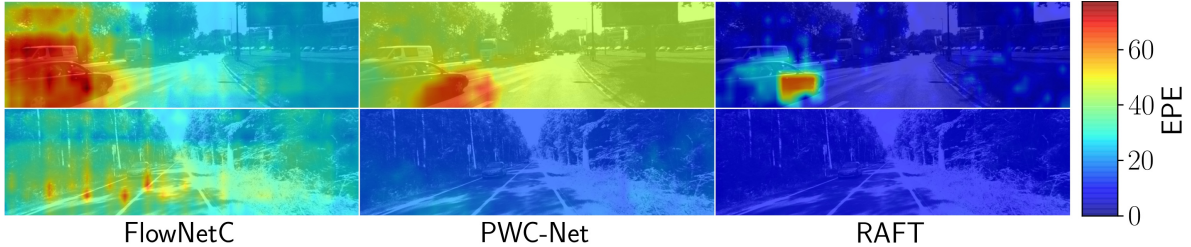


Figure 3: **Impact of spatial locations.** Effect of the spatial location of an optimized 102×102 patch. Best viewed in color.

the location with the highest attacked EPE. Figure 3 shows that the sensitivity to adversarial attacks depends much on the image and the location of the patch. The sensitivity of PWC-Net and RAFT can sometimes be high, as well. Especially image regions with large flow, *e.g.* fast moving objects, can lead to a severe deterioration of EPE. For the example in Figure 3 top row, worst case EPE deteriorates to 54.38, 38.95, and 65.61 for FlowNetS, FlowNet2 and SPyNet, respectively.

4.2. The Main Culprit: Correlation Layer

To analyze the features of flow networks during the attack, we visualize the unattacked and attacked features’ distributions using t-SNE [36] and compute the Maximum Mean Discrepancy (MMD) [13] between the two distributions. Comparing the FlowNetC’s feature embeddings with and without the attack reveals a large separation of the unattacked and attacked feature distributions after the correlation layer (Figure 4). Before the correlation layer the unattacked and attacked feature distributions are quite close together, whereas after the correlation they are in separate clusters in the t-SNE visualization. This is also indicated by the rapid increase of MMD from 0.246 to 3.331. On the other hand, the unattacked and attacked feature distributions of PWC-Net and RAFT are close to each other before and after applying the correlation layer and also the MMDs stay similar. Hence, we hypothesize that the correlation layer of FlowNetC is the main cause for the vulnerability to adversarial attacks.

To validate this hypothesis, we replaced attacked features with unattacked features. We used a 102×102 patch with uniform noise, pasted it at a random location and saved the feature maps. Afterwards, we attack FlowNetC with the adversarial patch of same size at the same location and replaced the attacked feature maps with the previously saved feature maps. Table 2 shows that fixing the correlation layer’s output features (corr) in this way removes the effect of the attack. Alternatively, fixing the features conv3(a,b) does the same. In contrast, fixing the features that bypass the correlation layer (conv_redir) keeps the attack fully effective. This clearly shows that the correlation layer is the root cause for the failure of the network.

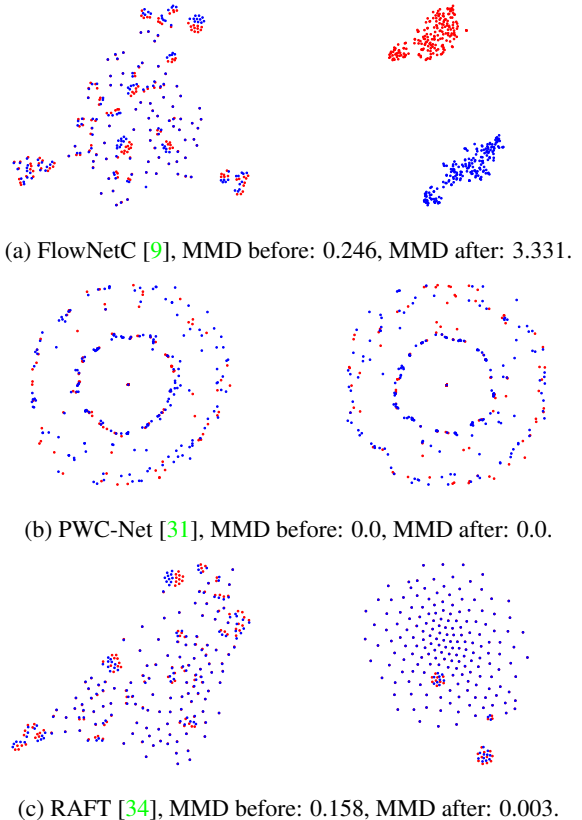


Figure 4: **t-SNE embeddings of features from FlowNetC, PWC-Net and RAFT.** Left: 2D embeddings of features before correlation layer. Right: 2D embeddings of features after correlation layer. We use our best found optimized adversarial 102×102 patch (2.1% of the image size). Blue and red points correspond to unattacked or attacked features, respectively. We visualize the 2D embeddings of features of PWC-Net and RAFT before or after applying the correlation layer for the first time. Note that a larger MMD indicates that the unattacked and attacked features are more separable. Best viewed in color and with zoom.

Replace features of	Without replacement	With replacement
conv3(a,b)	25.95	11.31
conv_redir	25.95	28.36
corr	25.95	12.67

Table 2: **Replacing attacked features.** Average EPE of the attacked FlowNetC (left) and the average EPE when the respective features are replaced by those from the unattacked FlowNetC on the KITTI 2015 training dataset using optimized and uniform noise 102×102 patches, respectively. See Figure 7 left for the encoder before the correlation layer in the original FlowNetC [9].

4.3. Relationship to the Aperture Problem

As we know that the correlation layer causes the sensitivity to adversarial attacks, there is good reason to suspect that this sensitivity arises from *self-correlations* within the adversarial patch. Indeed the optimized patch contains multiple self-similar patterns that lead to self-correlation. This means the patch triggers matching ambiguities that shows as a large active area in the correlation output. Successive layers that are supposed to interpret this output, successively spread the dominating ambiguous signals into the wider neighborhood, whereas the true correlation is outnumbered. This is related to the well-known aperture problem in optical flow, where repetitive patterns lead to an ambiguity in the optical flow and the receptive field (the aperture) determines the perceived motion.

However, why are other flow networks, such as PWC-Net or RAFT, which also have a correlation layer, much more robust to the attack? We suspect that the main reason for FlowNetC to be more sensitive w.r.t. patch-based adversarial attacks is less depth, resulting in a smaller receptive field before the correlation layer. More specifically, the larger receptive field size at the (first) correlation layer in PWC-Net and RAFT (631×631 and 106×106 vs. 31×31 for FlowNetC) sees also areas of the image that are not affected by the adversarial attack. RAFT in addition uses all-pairs correlation and correlation pooling, which further increases the effective receptive field size. This helps their correlation layer to keep the correlation peaked: the aperture is much larger than in FlowNetC.

5. Can We Attack Without Optimization?

As the attack is caused by ambiguities of a self-similar pattern in the correlation layer, it can also be created manually. To demonstrate this, we created a circular high-frequency black and white vertical striped patch; see Figure 5. Each stripe is two pixels wide. The pattern resembles those of psychophysical studies on the aperture problem.

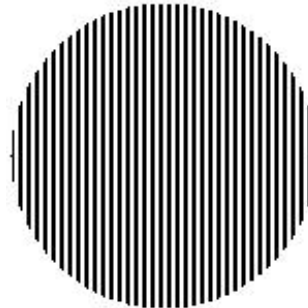


Figure 5: **Handcrafted patch.** Patch is enlarged for visualization.

Table 3 shows that FlowNetC is also vulnerable to this handcrafted patch, confirming again that the self-correlation in the correlation layer is the cause of the problem. The median performance of the other networks, also the Robust FlowNetC, is not affected, as they limit the effect of the ambiguous correlation signal to its local region or can even estimate the correct zero flow motion in this region. However, all flow networks are affected by the patch to some degree in the worst-case scenario, *i.e.*, when the patch is placed in the worst possible location in the image frames (Table 3 and Figure 6). However, this is hard to exploit in a physical attack and is similar to other optical flow estimation errors that naturally appear locally in some difficult image frames.

6. The Cure: Making FlowNetC Robust

Based on the previous analysis, we add corresponding architectural (and training improvements) to FlowNetC and show that this intervention also makes it robust to patch-based attacks. The components we add to FlowNetC, which is by far the most vulnerable network, are already included in most modern architectures and can be regarded as the important ingredients that make an optical flow network robust to repetitive patterns as used by patch-based adversarial attacks.

6.1. Architecture

We increase the receptive field before the correlation layer by adding (spatial resolution preserving) convolutional layers in each resolution level before the correlation layer. Moreover, we replace 5×5 convolutional layers in FlowNetC by 3×3 convolutional layers. This allows us to use deeper encoders with larger receptive field before the correlation layer and to stabilize the training. We call the FlowNetC variant with kernel size 3 and 4 convolutional layers per resolution level *Robust FlowNetC*, illustrated in Figure 7 right. For an ablation, we also created other variants of FlowNetC; see Table 4 for an overview of these variants.

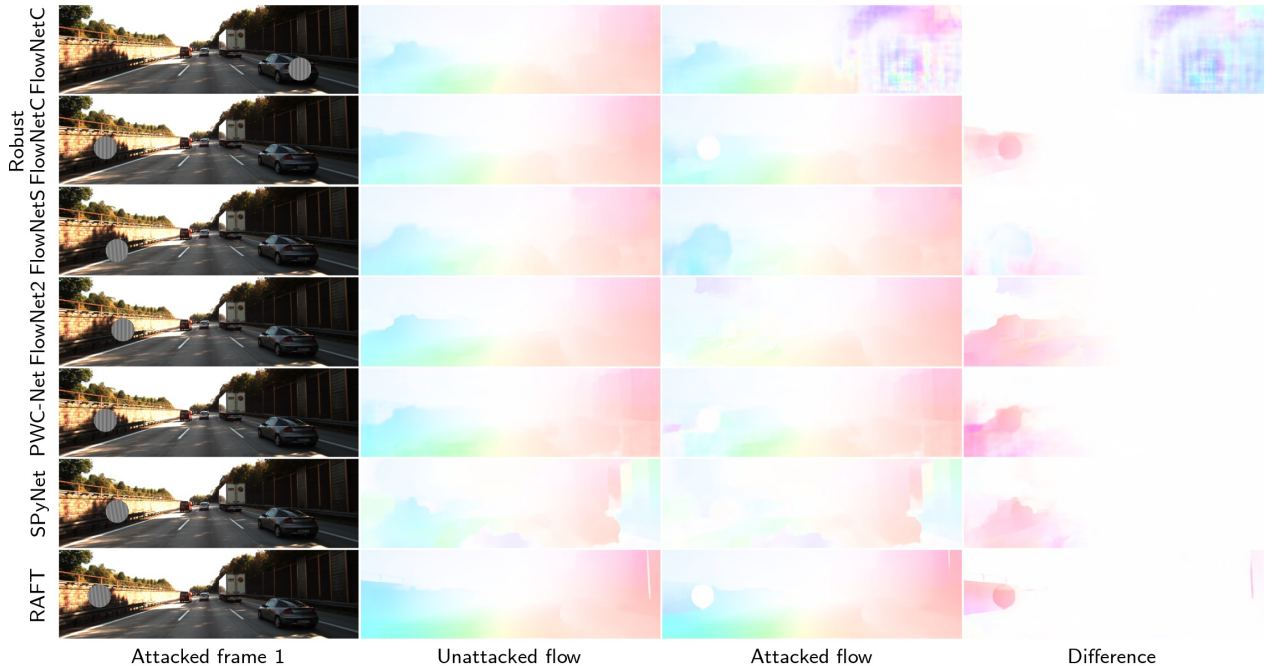


Figure 6: **Handcrafted patch attack.** 102x102 handcrafted patch attack on all flow networks. We show the patch at the worst possible spatial location for each flow network. Robust flow networks predict zero flow (white color) at the patch location (third column).

Flow Network	Unattacked EPE	25x25 (0.1%)		51x51 (0.5%)		102x102 (2.1%)		153x153 (4.8%)	
		Median	Worst	Median	Worst	Median	Worst	Median	Worst
FlowNetC [9]	11.50	11.66	16.66	15.81	29.08	23.41	46.12	30.97	52.27
Robust FlowNetC	9.95	9.95	11.14	9.86	11.74	9.60	13.08	9.27	13.64
FlowNetS [9]	14.33	14.35	15.66	14.50	17.00	14.64	20.10	14.55	22.32
FlowNet2 [17]	10.07	10.11	13.80	10.56	19.10	12.08	21.63	13.84	24.35
SPyNet [27]	24.26	24.22	26.24	24.06	27.41	23.28	27.46	22.20	26.62
PWC-Net [31]	12.55	12.54	14.82	12.45	16.10	12.02	16.87	11.42	16.26
RAFT [34]	5.86	5.80	7.08	5.74	7.44	5.49	8.69	5.17	8.96

Table 3: **Handcrafted patch attack.** Effect of handcrafted black and white striped patch (in pixel and percent of image size) on different flow networks. We show average median and worst case EPE over a coarse grid of spatial locations of the patch on the KITTI 2015 training dataset for each flow network.

6.2. Training Procedure

It has been shown that the training schedule is also important factor for good optical flow performance [17, 32]. Since we showed in the previous section that the patch-based attack is not a classical adversarial attack but simply makes the local estimation problem harder, stronger performance in general should also yield better robustness w.r.t. patch-based attacks. Hence, for the Robust FlowNetC we switch to the training pipeline of RAFT, *i.e.*, we use the AdamW optimizer [20], one cycle scheduler [29], gradient clipping, same augmentation pipeline and also initialize the weights of the models with Kaiming initialization [14]. Dif-

ferent to RAFT’s training procedure, we use a multiscale l_2 loss and pretrain on FlyingChairs [9] for 600k iterations with an initial learning rate of 10^{-4} . We then train on FlyingThings3D [22] for 300k iterations with a learning rate of 10^{-5} .

6.3. Evaluation

The impact of our simple architectural change can be clearly observed in Figure 6 and Table 3. We observe that Robust FlowNetC is significantly more robust w.r.t. patch-based adversarial attacks compared to the original FlowNetC. Additionally, in Figure 8, we visualize a more challenging scenario where the adversarial patch is allowed

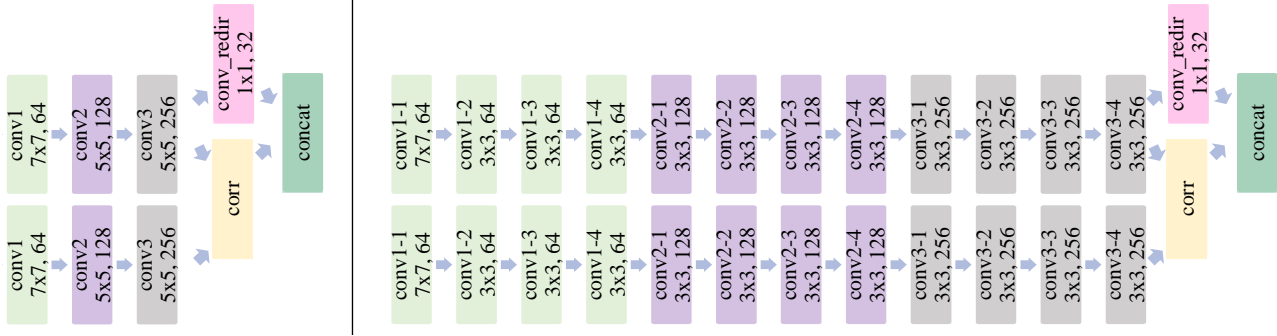


Figure 7: **Modified encoder before the correlation layer for Robust FlowNetC.** Left: original FlowNetC encoder [9]. Right: our Robust FlowNetC encoder. Blocks show the name, kernel size and number of filters. For Robust FlowNetC, the layers conv1-1, conv2-1 and conv3-1 are used for downsampling and hence have stride of 2.

Kernel size	Convs per resolution level	Receptive field
3	1	19
5	1	31
3	2	47
3	3	75
5	2	87
3	4	103

Table 4: **Overview over FlowNetC encoder variants.** The very first layer is always a 7×7 convolutional layer. See Figure 7 for visualizations of the original FlowNetC [9] and our Robust FlowNetC encoder.

to (freely) move between frames. From Figures 8 and 6, we can see that Robust FlowNetC correctly predicts the flow whether the patch moves or not between the two image frames. The patch has only a negligible impact on the surrounding image region, even if we move the patch between image frames. This small effect is because the patch makes the optical flow estimation problem harder, *e.g.*, due to occlusion, particularly since we show the worst-case placement of the patch. Figure 10 shows that the embeddings between the attacked and unattacked features are well-aligned – in contrast to the original FlowNetC.

Figure 9 shows by adding convolutional layers and thereby increasing the receptive field, as argued before, fixes the large sensitivity of the original FlowNetC. The ablation reveals the relationship between receptive field and robustness w.r.t. patch-based adversarial attacks. Note that the modifications not only improve the robustness w.r.t. patch-based attacks, but also improve the overall performance of the network.

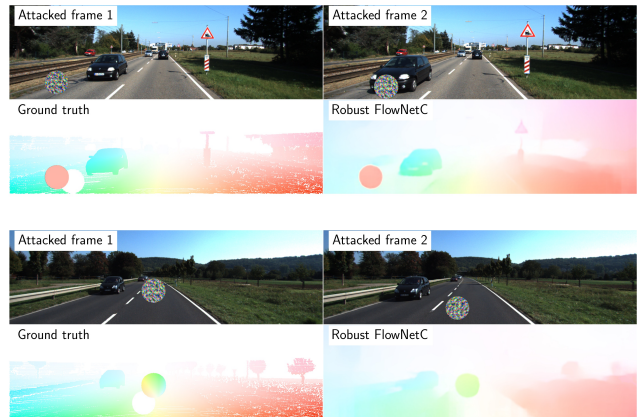


Figure 8: **Moving patch between image frames.** For each example block; top row shows attacked first and second image frame. Bottom row show ground truth and the predicted optical flow of Robust FlowNetC. We apply random affine transformations, *i.e.* translation, rotation and scaling, to the patch between the two images frames. Note that the patch can also move in the opposite direction w.r.t. its neighborhood, making it even more adversarial. Robust FlowNetC correctly estimates the optical flow. Note, however, that rotations of the patch are not estimated correctly and can lead to slight estimation errors of the motion of the patch.

7. Discussion

We have shown that self-similar patterns in conjunction with the correlation layer are the root cause of the vulnerability of optical flow networks to patch-based adversarial attacks. Self-similar patterns are a well-known problem for optical flow estimation and can be related to the aperture problem. In fact, we showed that a simple handcrafted self-similar patch has almost the same effect as an optimized adversarial patch.

As we understand the cause of the problem, there is a

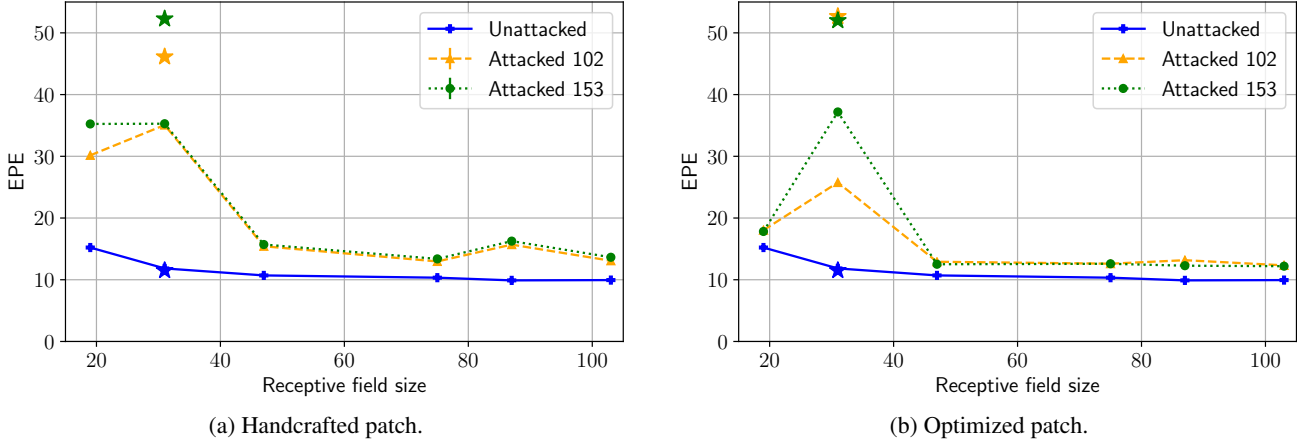


Figure 9: **Performance of FlowNetC variants with different receptive fields.** We show both unattacked and attacked worst case EPE. Left: handcrafted patch. Right: optimized patch. Stars show results for the original FlowNetC. For optimized patches, we show results using the patch with the highest attacked EPE after optimization over ten runs. Larger receptive fields reduce the attacked worst case EPE. We report the worst case attack w.r.t. location, *i.e.*, there remains a small gap between the attacked and the unattacked result, as for all networks; see Table 3. The two local peaks correspond to the variants with 5×5 filters; see Table 4.

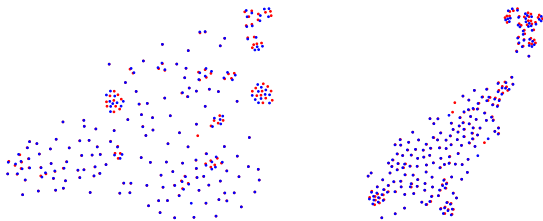


Figure 10: **t-SNE embedding of features from Robust FlowNetC.** Left: 2D embeddings of features before the correlation layer (MMD: 0.012). Right: 2D embeddings of features after the correlation layer (MMD: 0.007). Blue and red points correspond to unattacked or attacked features, respectively. Best viewed in color. In contrast to the original FlowNetC (Figure 4a), the attacked and unattacked embeddings stay well-aligned.

reliable way to prevent it: increasing the depth, and thereby increasing the receptive field size, such that the ambiguity caused by the self-similar pattern gets resolved. Many modern networks already have a deep encoder before the correlation layer with a large enough receptive field size, and, hence are robust to patch-based attacks. Thanks to our analysis, this is not simply coincidence or luck, but can be explained.

In this paper, we focused on patch-based attacks, which are particularly critical, since they can be used for physical attacks. However, the classical adversarial attack in recognition is a global white-box attack, where an imperceptible noise signal is added individually to each pixel. Wong *et*

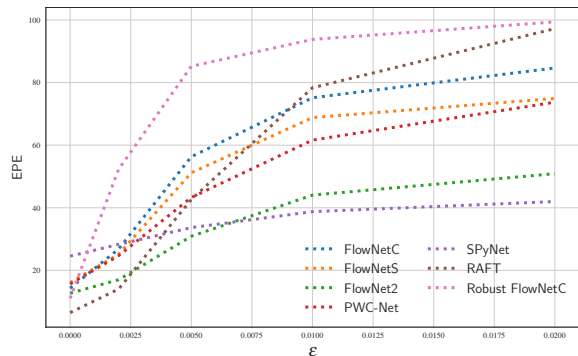


Figure 11: **Global, additive perturbation attack.** Iterative (Fast Gradient Sign Method) FGSM [18] significantly degrades optical flow performance for all flow networks.

al. [37] recently showed that also disparity networks are vulnerable to this attack. Figure 11 shows that, as expected, the same is true for optical flow estimation networks. It further shows that all networks – also those that are robust to patch-based attacks – are vulnerable to additive adversarial perturbations. The patch-based attack is only successful, if it can spread its influence into the larger neighborhood, which, as we showed, can be prevented. The global attack need not spread its poisonous influence but can focus on locally disturbing the matching process, as every pixel is perturbed. In practice, these attacks are less critical than patch-based attacks, but possibly also not completely harmless. Finding the cause for the vulnerability to these attacks will be the subject of future work.

Acknowledgements

We acknowledge funding by the German Research Foundation (BR 3815/10-1, INST 39/1108-1) and the German Ministry of Economics (KI Delta Learning). Gefördert durch das Bundesministerium für Wirtschaft und Energie aufgrund eines Beschlusses des Deutschen Bundestages.

References

- [1] Anish Athalye and Nicholas Carlini. On the robustness of the cvpr 2018 white-box adversarial example defenses. *arXiv*, 2018. 1, 2
- [2] Anish Athalye, Nicholas Carlini, and David Wagner. Obfuscated gradients give a false sense of security: Circumventing defenses to adversarial examples. In *ICML*, 2018. 2
- [3] Anish Athalye, Logan Engstrom, Andrew Ilyas, and Kevin Kwok. Synthesizing robust adversarial examples. In *ICML*, 2018. 2
- [4] M. J. Black and P. Anandan. The robust estimation of multiple motions: Parametric and piecewise-smooth flow fields. *CVIU*, 1996. 2
- [5] Tom B Brown, Dandelion Mané, Aurko Roy, Martín Abadi, and Justin Gilmer. Adversarial patch. *arXiv*, 2017. 2
- [6] Thomas Brox, Andrés Bruhn, Nils Papenberg, and Joachim Weickert. High accuracy optical flow estimation based on a theory for warping. In *ECCV*, 2004. 2
- [7] Thomas Brox and Jitendra Malik. Large displacement optical flow: descriptor matching in variational motion estimation. *IEEE Trans. PAMI*, 2010. 2
- [8] Nicholas Carlini and David Wagner. Adversarial examples are not easily detected: Bypassing ten detection methods. In *AISec Workshop*, 2017. 2
- [9] Alexey Dosovitskiy, Philipp Fischer, Eddy Ilg, Philip Hausser, Caner Hazirbas, Vladimir Golkov, Patrick Van Der Smagt, Daniel Cremers, and Thomas Brox. FlowNet: Learning optical flow with convolutional networks. In *ICCV*, 2015. 1, 2, 3, 4, 5, 6, 7, 12, 14, 17
- [10] Kevin Eykholt, Ivan Evtimov, Earlene Fernandes, Bo Li, Amir Rahmati, Chaowei Xiao, Atul Prakash, Tadayoshi Kohno, and Dawn Song. Robust physical-world attacks on deep learning visual classification. In *CVPR*, 2018. 2
- [11] Andreas Geiger, Philip Lenz, and Raquel Urtasun. Are we ready for autonomous driving? the kitti vision benchmark suite. In *CVPR*, 2012. 3, 11
- [12] Ian J Goodfellow, Jonathon Shlens, and Christian Szegedy. Explaining and harnessing adversarial examples. In *ICLR*, 2015. 2
- [13] Arthur Gretton, Karsten Borgwardt, Malte Rasch, Bernhard Schölkopf, and Alex Smola. A kernel method for the two-sample-problem. *NeurIPS*, 2006. 4
- [14] Kaiming He, Xiangyu Zhang, Shaoqing Ren, and Jian Sun. Delving deep into rectifiers: Surpassing human-level performance on imagenet classification. In *ICCV*, 2015. 6
- [15] Dan Hendrycks, Kevin Zhao, Steven Basart, Jacob Steinhardt, and Dawn Song. Natural adversarial examples. *CVPR*, 2021. 2
- [16] Berthold KP Horn and Brian G Schunck. Determining optical flow. *Artificial intelligence*, 1981. 2
- [17] Eddy Ilg, Nikolaus Mayer, Tonmoy Saikia, Margret Keuper, Alexey Dosovitskiy, and Thomas Brox. FlowNet 2.0: Evolution of optical flow estimation with deep networks. In *CVPR*, 2017. 2, 3, 6, 17
- [18] Alexey Kurakin, Ian Goodfellow, and Samy Bengio. Adversarial machine learning at scale. *ICLR*, 2017. 2, 8, 17
- [19] Yann A LeCun, Léon Bottou, Genevieve B Orr, and Klaus-Robert Müller. Efficient backprop. In *Neural networks: Tricks of the trade*. 2012. 2
- [20] Ilya Loshchilov and Frank Hutter. Decoupled weight decay regularization. In *ICLR*, 2019. 6
- [21] Aleksander Madry, Aleksandar Makelev, Ludwig Schmidt, Dimitris Tsipras, and Adrian Vladu. Towards deep learning models resistant to adversarial attacks. In *ICLR*, 2018. 2
- [22] Nikolaus Mayer, Eddy Ilg, Philip Hausser, Philipp Fischer, Daniel Cremers, Alexey Dosovitskiy, and Thomas Brox. A large dataset to train convolutional networks for disparity, optical flow, and scene flow estimation. In *CVPR*, 2016. 6
- [23] Moritz Menze and Andreas Geiger. Object scene flow for autonomous vehicles. In *CVPR*, 2015. 3, 11
- [24] Takeru Miyato, Shin-ichi Maeda, Masanori Koyama, and Shin Ishii. Virtual adversarial training: a regularization method for supervised and semi-supervised learning. *IEEE Trans. PAMI*, 2018. 2
- [25] Augustus Odena, Vincent Dumoulin, and Chris Olah. Deconvolution and checkerboard artifacts. *Distill*, 2016. 2
- [26] Nicolas Papernot, Patrick McDaniel, Xi Wu, Somesh Jha, and Ananthram Swami. Distillation as a defense to adversarial perturbations against deep neural networks. In *2016 IEEE symposium on security and privacy (SP)*, 2016. 2
- [27] Anurag Ranjan and Michael J Black. Optical flow estimation using a spatial pyramid network. In *CVPR*, 2017. 2, 3, 6, 17
- [28] Anurag Ranjan, Joel Janai, Andreas Geiger, and Michael J Black. Attacking optical flow. In *ICCV*, 2019. 1, 2, 3, 11, 12
- [29] Leslie N Smith and Nicholay Topin. Super-convergence: Very fast training of neural networks using large learning rates. In *Artificial Intelligence and Machine Learning for Multi-Domain Operations Applications*, 2019. 6
- [30] Jiawei Su, Danilo Vasconcellos Vargas, and Kouichi Sakurai. One pixel attack for fooling deep neural networks. *IEEE Transactions on Evolutionary Computation*, 2019. 2
- [31] Deqing Sun, Xiaodong Yang, Ming-Yu Liu, and Jan Kautz. Pwc-net: Cnns for optical flow using pyramid, warping, and cost volume. In *CVPR*, 2018. 2, 3, 4, 6, 17
- [32] Deqing Sun, Xiaodong Yang, Ming-Yu Liu, and Jan Kautz. Models matter, so does training: An empirical study of cnns for optical flow estimation. *IEEE Trans. PAMI*, 2019. 6
- [33] Christian Szegedy, Wojciech Zaremba, Ilya Sutskever, Joan Bruna, Dumitru Erhan, Ian Goodfellow, and Rob Fergus. Intriguing properties of neural networks. In *ICLR*, 2014. 2
- [34] Zachary Teed and Jia Deng. Raft: Recurrent all-pairs field transforms for optical flow. In *ECCV*, 2020. 2, 3, 4, 6, 17
- [35] Jonathan Uesato, Brendan O’donoghue, Pushmeet Kohli, and Aaron Oord. Adversarial risk and the dangers of evaluating against weak attacks. In *ICML*, 2018. 2

- [36] Laurens Van der Maaten and Geoffrey Hinton. Visualizing data using t-sne. *Journal of Machine Learning Research*, 2008. [4](#), [11](#)
- [37] Alex Wong, Mukund Mundhra, and Stefano Soatto. Stereopagnosia: Fooling stereo networks with adversarial perturbations. In *AAAI*, 2021. [2](#), [8](#), [11](#)
- [38] Han Xu, Yao Ma, Hao-Chen Liu, Debayan Deb, Hui Liu, Ji-Liang Tang, and Anil K Jain. Adversarial attacks and defenses in images, graphs and text: A review. *International Journal of Automation and Computing*, 2020. [1](#)

Supplementary Material

A. Additional Evaluation Details for Different Attacks

In the following, we provide further details on different attacks and their evaluation for completeness. In all our experiments, we always use pre-trained models *without* fine-tuning on the KITTI dataset.

For patch-based attacks, we follow the attacking and white-box evaluation procedure of Ranjan *et al.* [28]. We optimize a circular patch by optimizing w.r.t. Equation 1 using flow network’s predictions as pseudo ground truth from raw KITTI [11] for optimization and the annotated images as validation set. We use scale augmentation within $\pm 5\%$, rotation augmentation within $\pm 10^\circ$ and randomly paste the patch at different image locations, but at the *same* location in both image frames.

For experiments, we use the KITTI 2015 training set [23] and resize images to 384×1280 . During the attack, we paste the patch also at the *same* location in both image frames, if stated not otherwise. We always compute unattacked and attacked EPE and set the region of the ground truth which the patch occludes to zero motion. For the computation of the spatial location heat map, we move the patch in strides of 25 pixels in x - and y -direction. For the t-SNE [36] plots, we extracted the feature maps from the flow networks and computed the mean over the spatial dimensions to reduce the dimensionality of the feature maps. For the experiment with Robust FlowNetC and its variants, we optimized > 20 or 10 adversarial patches with different learning rates for each patch size, respectively. We chose the three worst patches in terms of attacked EPE on the validation set and computed the spatial location heat map to get the worst case attacked EPE. We also chose more patches, but these other patches were not as effective as the three worst patches. Finally, we also tested moving the patch between image frames. For this we randomly sampled translation within ± 50 , full rotation (*i.e.* $\pm 180^\circ$) and scale augmentation within $\pm 5\%$.

For global attacks, we use the same procedure as Wong *et al.* [37], but we only use pre-trained models *without* fine tuning on the KITTI dataset and minimize the cosine similarity as for patch-based attacks. We use the KITTI 2015 training set [23] for attacking and evaluation and resize images to 256×640 due to computational limitations. We also use the same upper norms $\epsilon = \{0.02, 0.01, 0.005, 0.002\}$ and momentum $\beta = 0.47$, but use the same learning rate $\alpha = 0.002$ for all upper norms.

B. Visual Examples for Handcrafted Attacks

In Figure 1 we show additional qualitative results for the circular high-frequency black and white vertical striped patch on FlowNetC. We only show results for FlowNetC, since it is the most vulnerable flow network and thus shows the most severe effect in the optical flow estimates. Similar to the optimized patch, the handcrafted patch severely deteriorates the optical flow estimates.

C. Ablations for Handcrafted Attacks

We conducted several ablations to identify the main ingredients for a successful attack with the handcrafted patch besides its self-similar pattern. We used FlowNetC as the flow network for the ablations because it is the most sensitive w.r.t. the patch-based attacks. We tested the influence of the contrast between the stripes. For that we fix the black or white color of the handcrafted patch and change each other color to change the contrast between the stripes. Figure 2 shows larger contrast between the stripes causes more severe deterioration of optical flow performance. Interestingly, we can see an exponential increase in worst case attacked EPE as we increase the contrast between the stripes. The colors of the patch are another ingredient (Figure 3) of the handcrafted patch. The handcrafted self-similar pattern also works when we use different colors. However, note that the effect of the handcrafted patch may be less severe for different color patterns. Also observe that regions with zero flow are more sensitive w.r.t. patch-based attacks. Figure 4 shows that thin stripes are also an important ingredient. Finally, we also tested the effect of the rotational orientation of the patch. Figure 5 shows that the rotational orientation of the patch is also an important ingredient for a successful attack. Interestingly, we observe that the self-similar pattern causes a stronger degradation of the optical flow performance when oriented in axial directions.

D. Increasing the Receptive Field Size by Increasing the Dilation Rate

We also tried to increase the receptive field by increasing the dilation rate of the convolutional layers of FlowNetC’s encoder. We used dilation rates $\{1, 2, 4, 8\}$, where a dilation rate of 1 corresponds to the original FlowNetC. Figure 6 shows that increasing the dilation rates also makes FlowNetC more robust w.r.t. patch-based attacks. The gap between unattacked and attacked EPE can be mostly attributed to occlusions causing optical flow performance to deteriorate. More specifically, for the FlowNetC variant

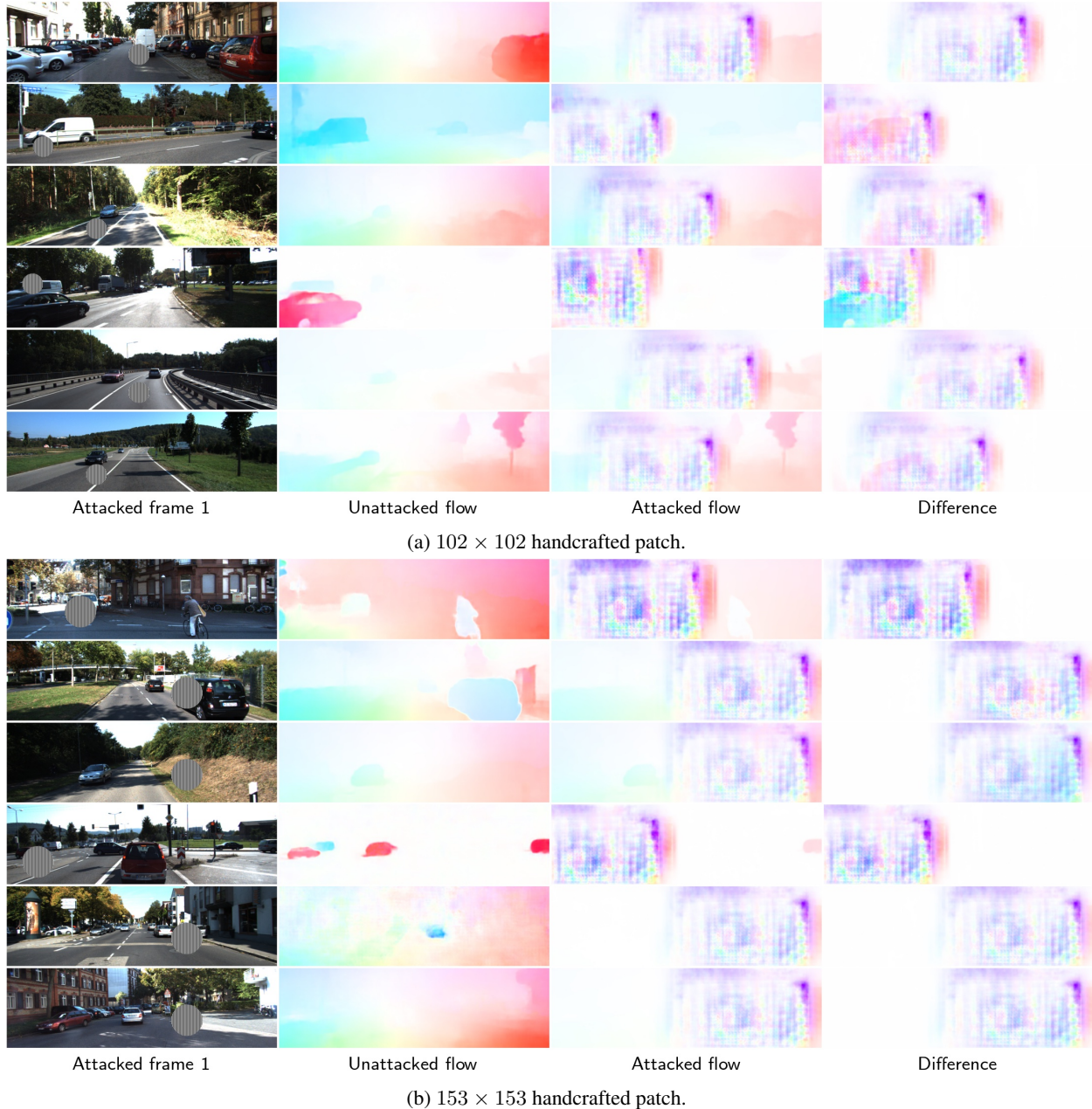


Figure 1: **Additional qualitative examples for handcrafted patch.** We show the handcrafted patch at the worst possible spatial location for FlowNetC [9]. The handcrafted patch leads to severe deteriorations of the optical flow estimates. Best viewed in color.

with dilation rate 8 a 102×102 and 153×153 patch with uniform noise has EPE of 23.32 or 22.3, respectively. This is similar to the worst-case attacked EPEs for the handcrafted and optimized patches. However, the optical flow performance deteriorates significantly when the dilation rate is increased. Therefore, increasing the receptive field by adding more depth is preferable to make flow networks more robust w.r.t. patch-based attacks.

E. Realistic Motion of Patches

We also tried to use realistic motion of patches by considering them as part of the static scene, as described by Ranjan *et al.* [28]. We found that it has a negligible effect w.r.t. the worst case attacked EPE for Robust FlowNetC, *i.e.*, 12.16 and 12.11 to 13.60 and 14.57 for 102×102 or 153×153 patches, respectively. The higher worst case at-

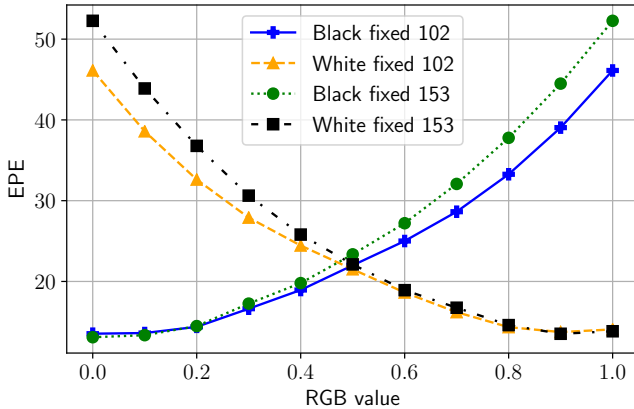


Figure 2: **Contrast between stripes.** We keep the black or white color of the black and white vertical striped patch fixed and move the other color towards black and white, respectively. We attack with those variant of the handcrafted patch FlowNetC. We observe that the contrast between the stripes is an important ingredient for a successful attack with the handcrafted patch. Interestingly, worst case attacked EPE increases exponentially with contrast.

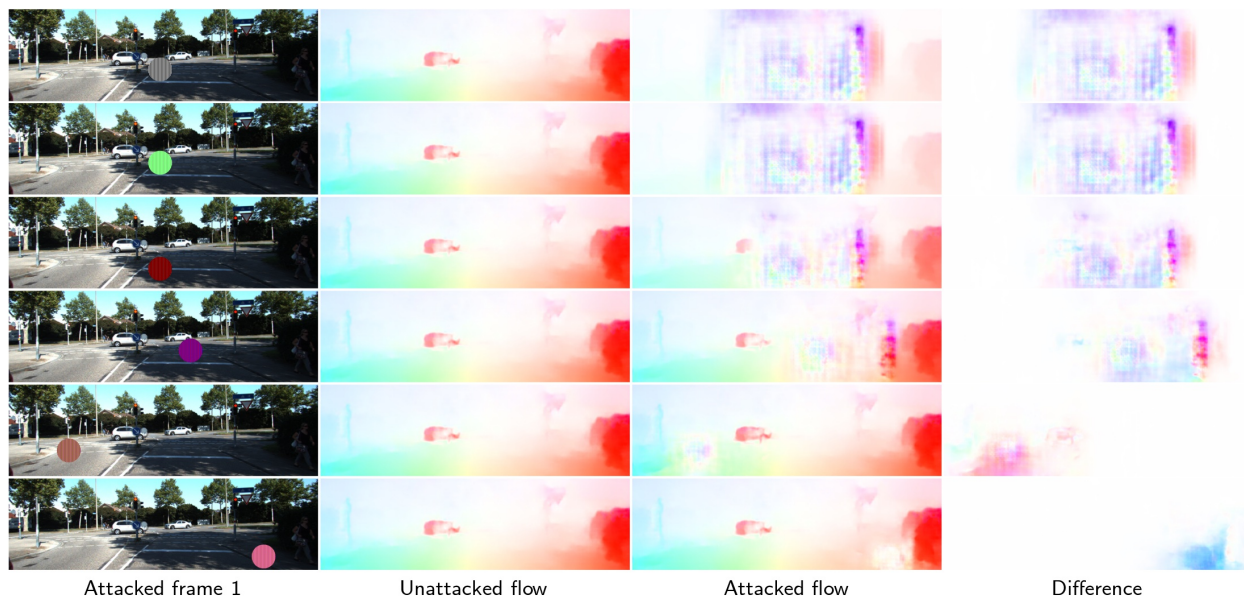
tacked EPEs can be explained by the fact that the patches were mostly placed in the boundary regions of the first image frame at the worst case spatial location, so that they disappeared in the second image frame.

F. Visual Examples for Robust FlowNetC

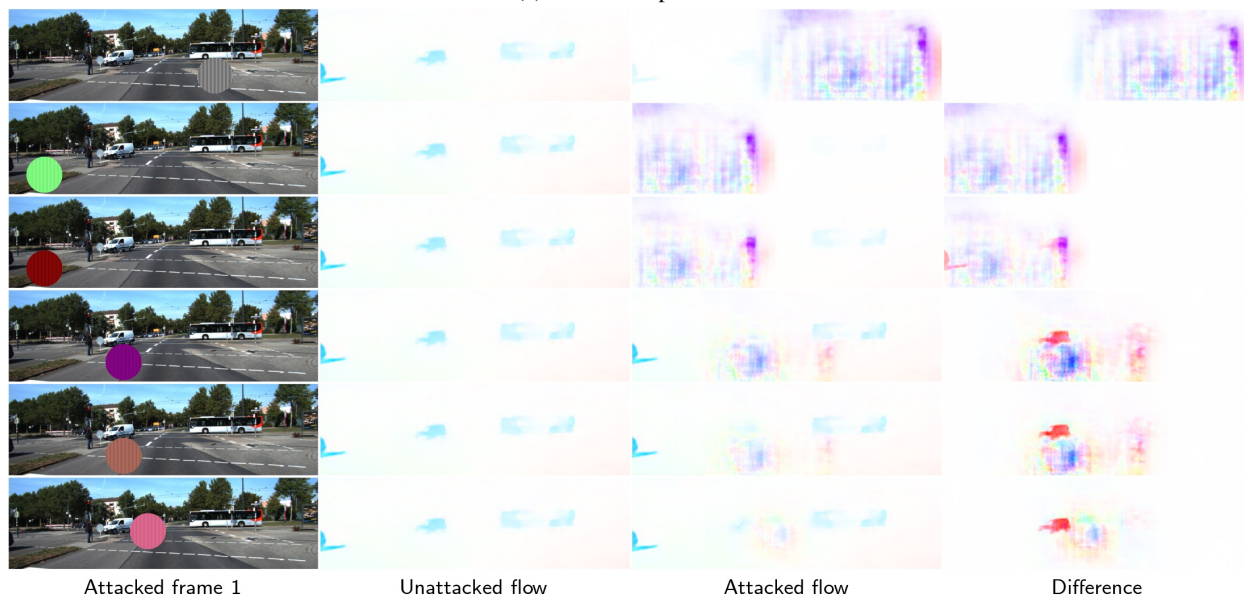
In Figure 7 we show additional qualitative results for patch-based adversarial attacks on Robust FlowNetC. Robust FlowNetC significantly improves robustness w.r.t. patch-based adversarial attacks. However, as with other flow networks, we would like to emphasize that there are some particular hard image frames that can cause severe deterioration of optical flow performance.

G. Visual Examples for Global Attacks

In Figure 8 we show qualitative results for global, additive perturbation attacks on different flow networks. As expected, we see severe deterioration of the optical flow estimates across all flow networks. Especially homogeneous flow areas seem to be sensitive to the perturbations.



(a) 102×102 patches.



(b) 153×153 patches.

Figure 3: **Different colors.** We use the same self-similar pattern, but use different color pairs. From top to bottom for each subfigure: black-white, green-white, red-black, red-blue, green-violet and violet-orange. We show each handcrafted patch at the worst possible spatial location for FlowNetC [9]. We observe that the attack also works with different color pairs. However, for some color pairs the effect of the patch is less severe. Best viewed in color.

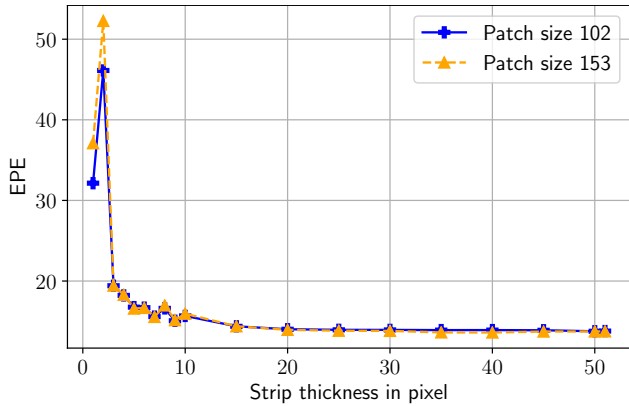


Figure 4: **Strip thickness.** We alter the thickness of the stripes and attack FlowNetC. We observe that high-frequency of the self-similar pattern is an important ingredient for a successful attack.

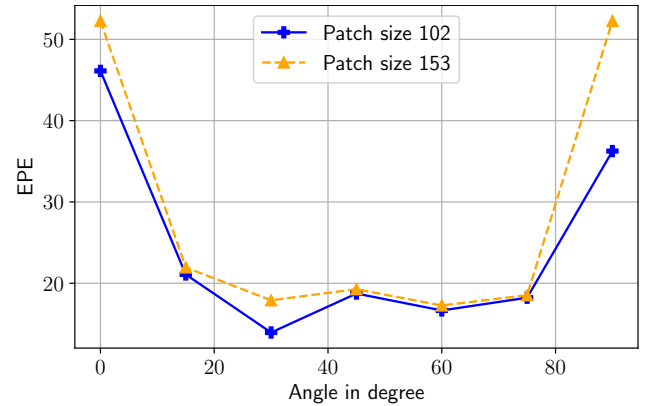
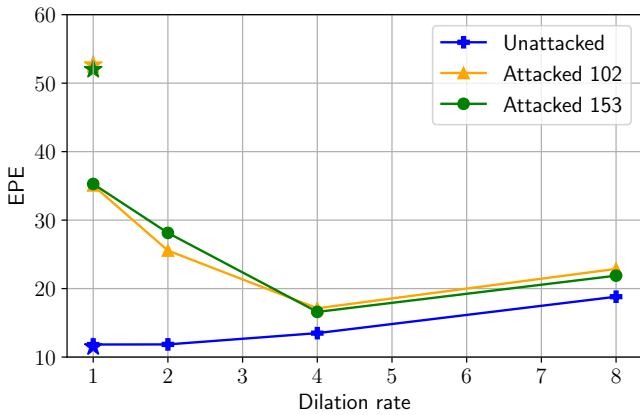
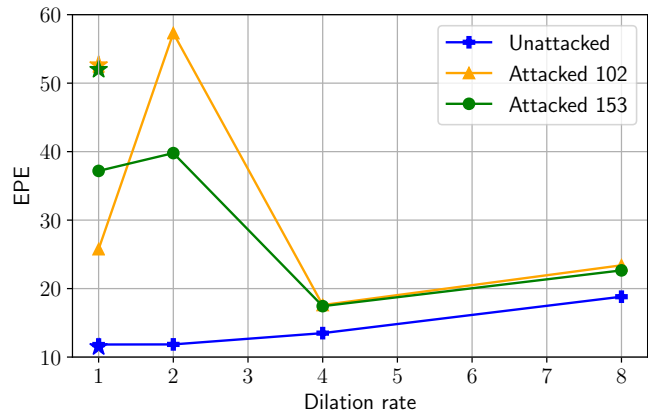


Figure 5: **Rotational orientation.** We rotate the hand-crafted patch and attack FlowNetC. Rotational angle of 0° corresponds to vertical stripes and rotational angle 90° corresponds to horizontal stripes. We observe an U-shaped form of worst case attacked EPE. This indicates that the stripes oriented in the axial direction cause more deterioration of optical flow performance.

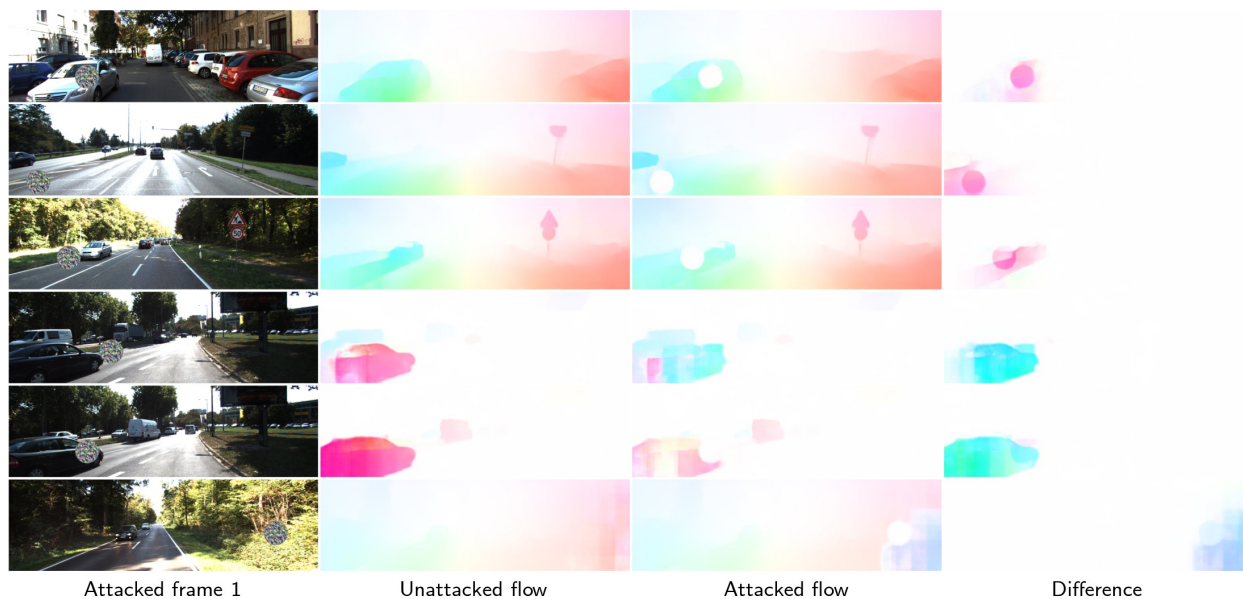


(a) Handcrafted patch.

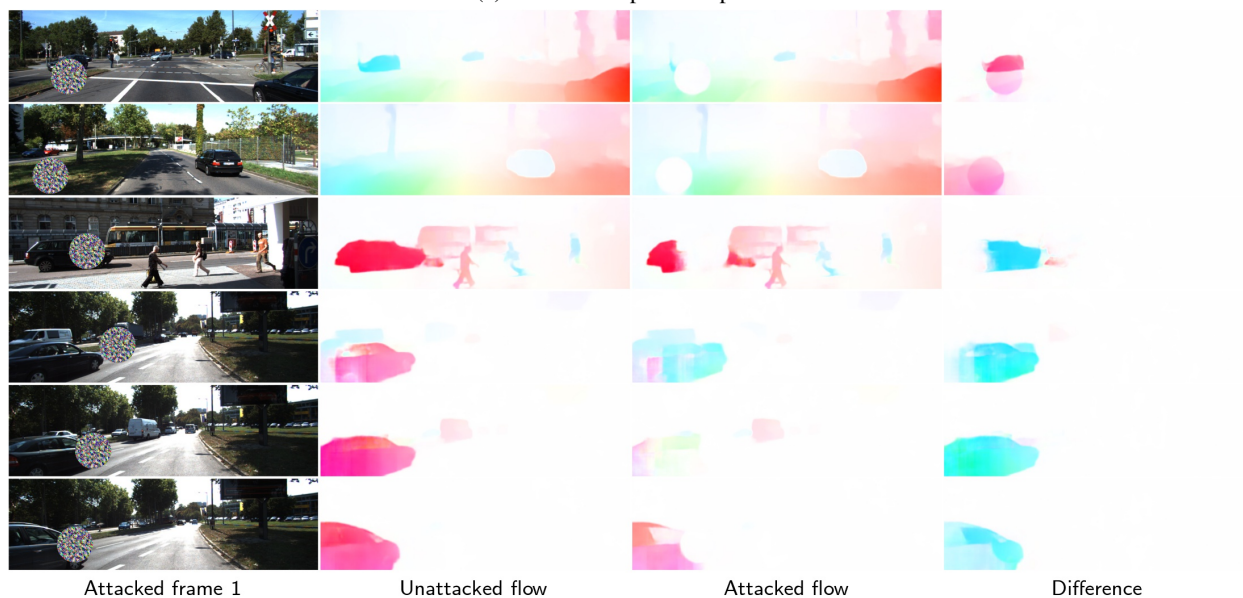


(b) Optimized patch.

Figure 6: **Performance of FlowNetC variants with different dilation rates.** We show both unattacked and attacked worst case EPE. Left: handcrafted patch. Right: optimized patch. Stars show results for the original FlowNetC. For optimized patches, we show results using the patch with the highest attacked worst case EPE after optimization over ten runs. Increasing the dilation rate also improves the robustness w.r.t. patch-based, adversarial attacks. However, overall optical flow performance deteriorates.



(a) 102×102 optimized patch.



(b) 153×153 optimized patch.

Figure 7: **Additional qualitative examples for Robust FlowNetC.** We show the best found optimized patch at the worst possible spatial location for Robust FlowNetC. The bottom three rows of each subfigure show the worst samples w.r.t. the greatest absolute degradation of worst case attacked EPE in descending order. Best viewed in color.

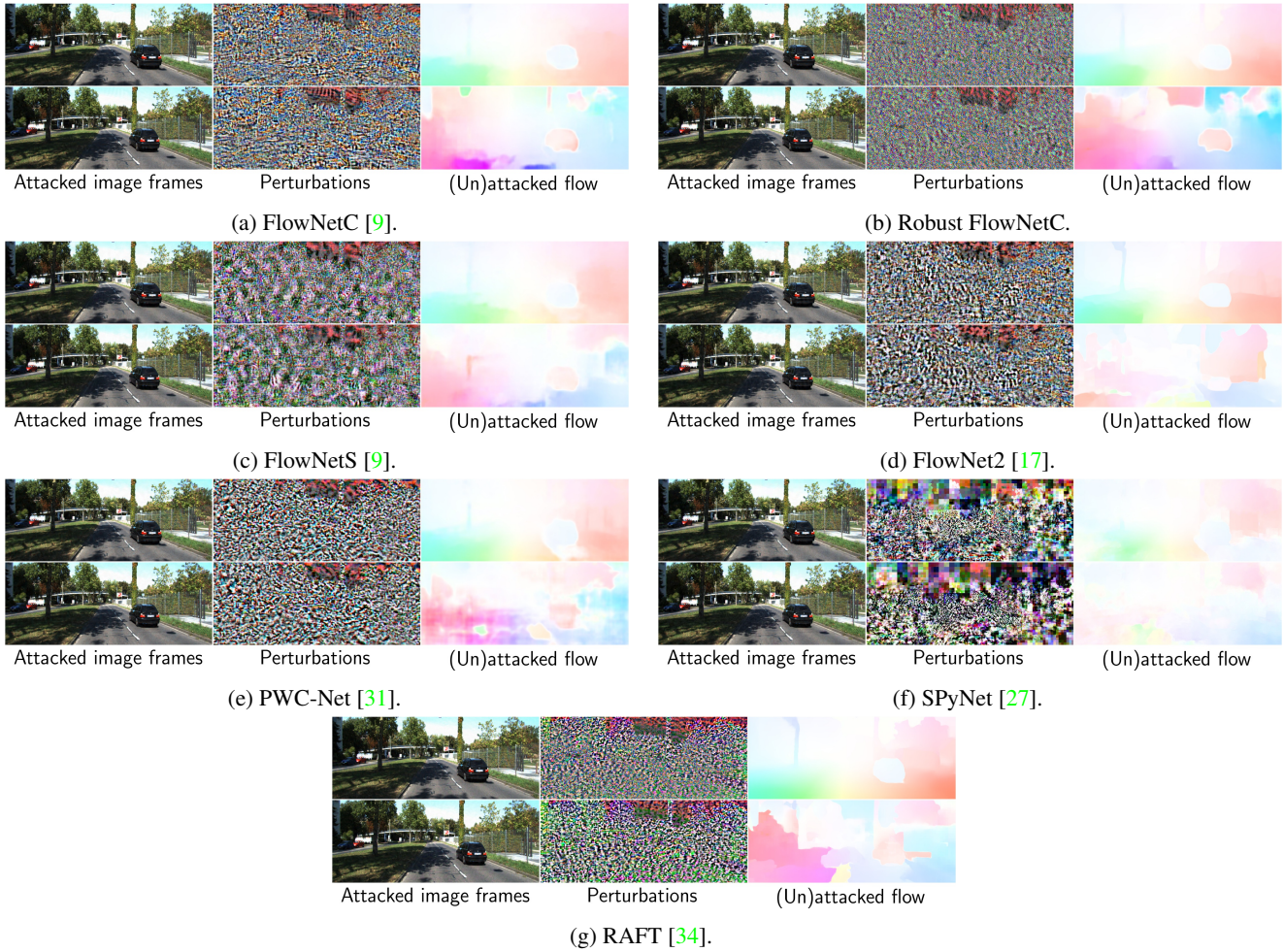


Figure 8: **Global, additive perturbation attacks.** Global, additive perturbation attacks on different flow networks. In each subfigure, we show in the first row the attacked first frame with perturbation, the perturbation of the first frame and the unattacked flow estimate, and in the second row the attacked second frame with perturbation, the perturbation of the second frame and the attacked flow estimate. Iterative (Fast Gradient Sign Method) FGSM [18] with upper norm $\epsilon = 0.02$ significantly degrades optical flow estimates for all flow networks. Note that homogeneous optical flow regions in particular are subject to the perturbation attack. Best viewed in color.